# Variations in Weld Ferrite Content Due to P and S

*P and S increase the ferrite content of welds containing the lathy ferrite morphology but slightly decrease the ferrite content of welds containing regions of primary austenite solidification*

BY J. A. BROOKS, A. W. THOMPSON, AND J. C. WILLIAMS

ABSTRACT. It was found that additions of P and S can have a considerable effect on the amount of weld ferrite in Fe-Ni-Cr austenitic alloys. These impurities significantly increased the ferrite content of welds containing primarily the lathy ferrite morphology, but slightly decreased the ferrite content of welds containing regions of primary austenite solidification. The reduction in ferrite is explained in terms of Cr-enriched inclusions decreasing the Cr equivalent and ferrite content.

In an alloy with welds containing skeletal ferrite in which the ferrite → austenite transformation is also important, S slightly decreased the measured ferrite content while P slightly increased it. It was concluded that reduced interphase boundary mobility resulted from P and S during the solid-state diffusion-controlled transformation of ferrite → austenite. This decreased boundary mobility resulted in a reduction of the extent to which austenite consumed the ferrite, which increased the ferrite content especially in the lathy ferrite morphology of primary ferrite solidified welds.

*J. A. BROOKS, former Graduate Fellow at Carnegie-Mellon University, is with Sandia National Laboratories, Livermore, California; A. W. THOMPSON and J. C. WILLIAMS are Professors of Metallurgy and Materials Science, Carnegie-Mellon University, Pittsburgh, Pennsylvania.*

## Introduction

The correlation between ferrite content and hot cracking in austenitic stainless steel welds has been recognized for many years. Since some of the early work by Scherer, *et al.* (Ref. 1), showing the beneficial effect of 5-35% ferrite in reducing cracking, many investigations have been aimed at predicting weld ferrite

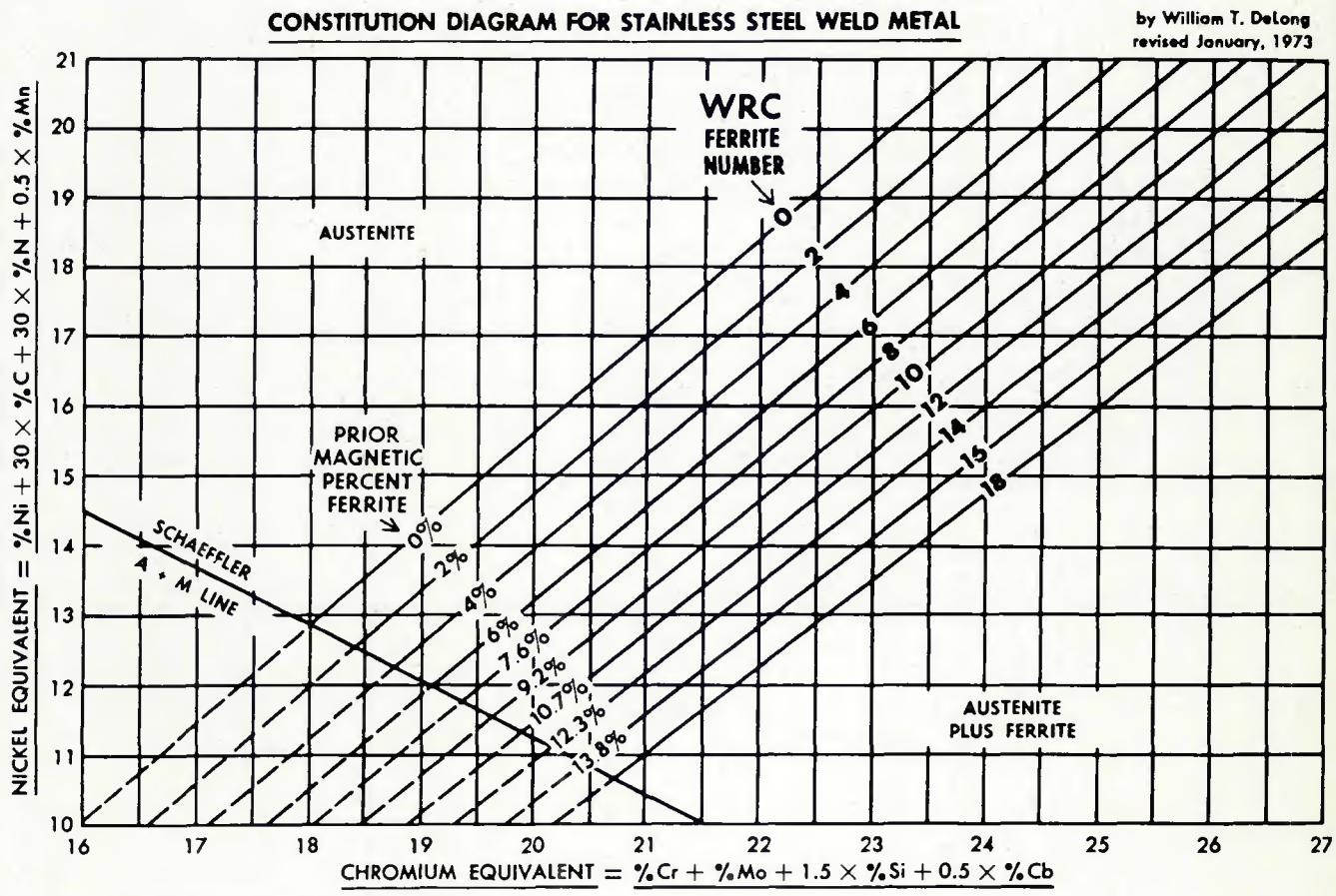


*Fig. 1—DeLong diagram used for predicting weld ferrite from alloy composition*

Table 1—Experimental Base Metal Alloy Composition, Wt-%

| Base metal alloy | Cr | Ni | Si | C | N | P | S | Fe |
|---|---|---|---|---|---|---|---|---|
| 19-11 | 18.67 | 11.34 | .01 | .009 | .003 | .002 | .003 | bal |
| 22-13 | 21.87 | 13.05 | .01 | .016 | .003 | .004 | .004 | bal |
| 23-12 | 22.81 | 11.92 | .01 | .010 | .004 | .003 | .003 | bal |

content from alloy chemistry (Ref. 2). Probably the most familiar diagram used to predict ferrite content is that published by Schaeffler (Ref. 3) in 1949. Revised diagrams have since been published that have improved accuracy or include additional alloying elements such as the diagram by DeLong, *et al.* (Ref. 4) shown in Fig. 1. With these diagrams, one may predict the as-deposited weld ferrite content by plotting the $Cr_{eq}$ and $Ni_{eq}$ (Cr and Ni equivalents) calculated from heat chemistry. As shown in Fig. 1, C, N, and Mn are included in the $Ni_{eq}$ while Mo, Si, and Nb are included in the $Cr_{eq}$. In a more recent diagram published by Hull (Ref. 5), it is shown that Co and Cu act as Ni equivalents while V, W, Ti, Ta and Al act as Cr equivalents. Values of the multiplication factors of the $Ni_{eq}$ and $Cr_{eq}$ were determined using a regression analysis.

It has been further shown that as the P and S contents of welds increase, the amount of ferrite required to eliminate cracking also increases (Ref. 6,7). Furthermore, what may be of equal or greater importance than the actual ferrite content in determining the cracking susceptibility, is the structure of primary solidification (Ref. 8,9). The primary solidification, *i.e.*, the first solid to form from the melt, may be either ferrite or austenite. This depends generally upon which side of the Fe-Ni-Cr ternary eutectic trough the nominal composition lies.

An investigation was conducted to increase understanding of the complex relationships which determine weld hot cracking susceptibility (Ref. 10). The portion of the investigation reported here involves the doping of Fe-Ni-Cr ternary alloys with different levels of P and S. Of concern was the extent to which the impurity additions could affect weld ferrite content. The welds evaluated and reported here were obtained from spot Varestraint (Ref. 11) test specimens doped with varying impurity levels.

## Materials and Testing

Materials used in this study were Fe-Ni-Cr ternary alloys. The composition of these alloys is shown in Table 1, where the alloy designation corresponds to the Cr and Ni contents. When welded, these alloys exhibit a wide range of microstructures. The different solidification behaviors and resulting ferrite morphologies have been shown schematically by Kujanpää, *et al.* (Ref. 12). A modification of their schematics in which some details have been modified or idealized is shown in Fig. 2. Alloy 23-12 solidifies largely as ferrite which transforms to a lathy ferrite morphology on cooling with a retained ferrite content of FN ~22. The lathy ferrite structure characteristic of welds of this alloy is shown schematically in Fig. 2.

Alloy 22-13 also solidifies as primary ferrite but with a larger fraction of secondary austenitic solidification. As-welded microstructures contain mainly the skeletal ferrite morphology with a ferrite content of FN ~8. The skeletal ferrite characteristic of welds in this alloy is also shown in the schematic of Fig. 2.

Alloy 19-11 when welded has a FN ~3 but was observed to solidify in a mixed mode—that is, some regions solidified as primary ferrite while other regions solidified as primary austenite, in which case the ferrite is a product of the eutectic reaction occuring during the last stages of solidification. This eutectic ferrite is then present along cell boundaries, unlike the skeletal and lathy ferrite morphologies, in which the ferrite is contained mainly within the cell cores. The microstructure of welds in this alloy can then be characterized by regions of both the eutectic ferrite and skeletal ferrite of Fig. 2.

Representative microstructures of welds of the three different alloys are shown in Fig. 3. A micrograph of alloy 19-11 is shown in Fig. 3A. A region of primary austenite solidification is at the left of the micrograph, while a region of primary ferrite solidification is at the right. The typical microstructure of the Varestraint welds of alloy 22-13 is shown in Fig. 3B. Small, spherical sulfide particles are visible in addition to the skeletal ferrite. A micrograph of alloy 23-12 is shown in Fig. 3C. Lathy ferrite is visible along the cell core, while sulfide particles are visible along the cell boundaries; the sulfides resulted from high S additions.

Disagreement exists in the literature as to the nature of the solid state transformations which result in the different ferrite morphologies of primary ferrite solidified welds (Fig. 2). Some workers have suggested that the transformations are diffusionless (Ref. 13-16) while others suggest that different ferrite morphologies are a result of diffusion-controlled transformations (Ref. 17-20). Extensive TEM (transmission electron microscopy) and STEM (scanning TEM) studies of these different structures have clearly shown that the transformations are diffusion-controlled with extensive partitioning of Cr to the ferrite and Ni to the austenite (Ref. 10,21-24).

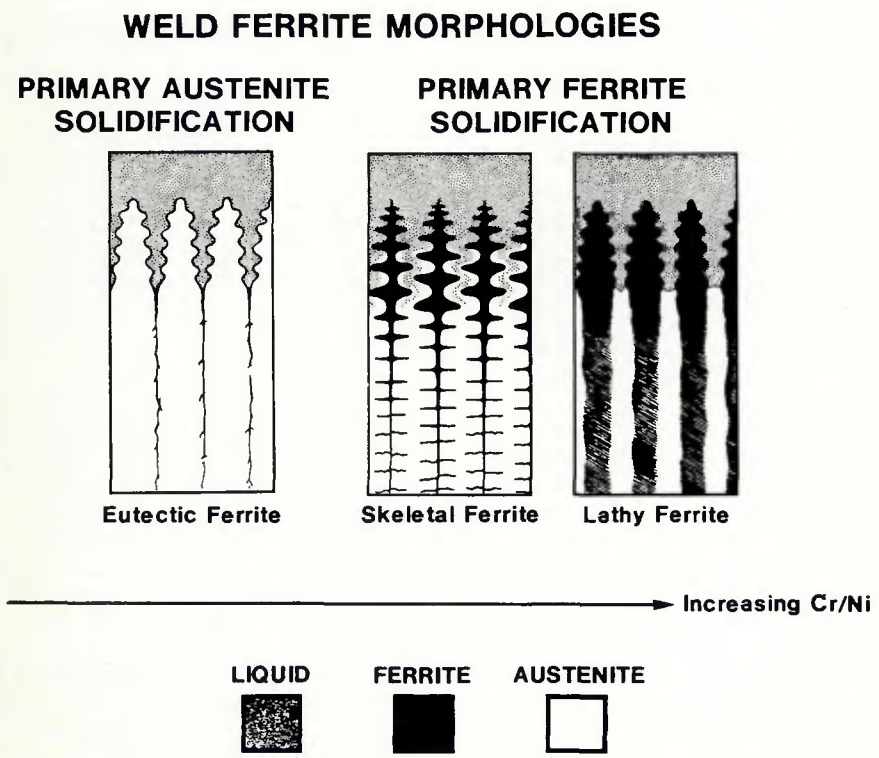


*Fig. 2—Schematic of solidification behavior and ferrite morphologies. Note the solid state transformations following primary ferrite solidification*

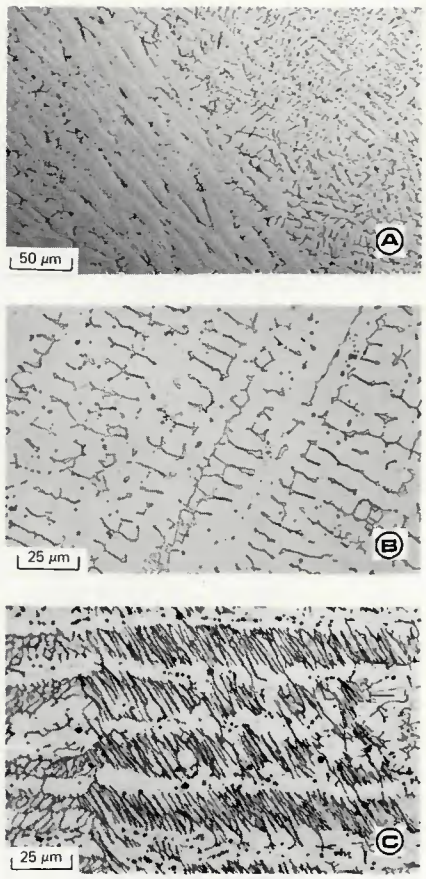


*Fig. 3 — Weld microstructures of alloys used in this study: A — mixed eutectic ferrite (left) and skeletal ferrite (right) typical of alloy 19-11; B — skeletal ferrite typical of alloy 22-13; C — lathy ferrite along cell core of alloy 23-12. Small spherical particles in cell boundaries of B and C are sulfides*

Ferrite measurements were made on impurity-doped welds of spot Varestraint test specimens used for determining cracking susceptibility (Ref. 10). This testing technique is described elsewhere (Ref. 11). A ~ 1.6 mm (0.06 in.) diameter hole ~ 1.6 mm (0.06 in.) deep was drilled in the center of the 2.22 × 0.64 × 15.24 cm (⅞ × ¼ × 6 in.) test specimen. The holes were filled with either FeS or FeP powders. The amount of P and S was determined by weighing the sample before and after the powder addition.

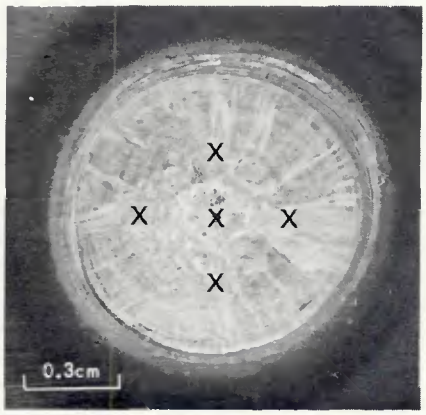


*Fig. 4 — Typical weld showing regions at which Magne-gage measurements were taken for ferrite determination*

The powders were fused in the specimen using manual GTA welding with low welding current. This fused region was only ~ 10% of the size of the final Varestraint spot weld. The final Varestraint spot welds were ~ 9.5 mm (⅜ in.) in diameter and ~ 2.4 mm (0.094 in.) deep. The ferrite content of the spot weld was measured with a Magne-gage in four regions ~ 90 deg apart. The readings were made between the center and edge of the GTA spot weld fusion zone.

A typical Varestraint weld is shown in Fig. 4. The "X" 's indicate the five regions at which the Magne-gage readings were taken to determine the average ferrite content. Impurity content was estimated from the weight of powder addition and weld volume. The differences between this estimated value and the chemical analysis of some of the actual welds are compared in Table 2.

## Ferrite Measurement Results

Results of ferrite measurements are shown in Fig. 5. As shown, increasing P and S slightly decreased the measured ferrite content of alloy 19-11; in general, S had a more potent effect than P.

In alloy 23-12, the measured FN of the Varestraint welds with low impurity additions was less than that in bead-on-plate GTA welds. This may be related to the effect of solidification and cooling rates on ferrite content (Ref. 24,25). However, as shown, both P and S significantly increased the ferrite level; the measured ferrite content increased from FN ~ 14 at 0.06% impurity level to FN ~ 18 at 0.15%.

The ferrite content of alloy 22-13 changed only slightly with impurity addition. However, P additions appeared to increase the ferrite content slightly, while at high levels of S, ~ 0.15%, the measured ferrite content was decreased from 8 to 6.

## Impurity-Doped Weld Microstructures

Detailed TEM and STEM studies were conducted on impurity partitioning and segregation (Ref. 10) and are to be more thoroughly discussed in a later publication. Here, only those structures are summarized which facilitate the understanding of the observed ferrite variations.

Chromium sulfide particles were observed in all welds doped with S. These particles, ~ 0.5 μm in diameter, appeared from both TEM and STEM analysis to be CrS. Such particles, in welds containing the different ferrite morphologies, are shown in the TEM micrographs of Fig. 6. Figure 6A shows particles along the eutectic ferrite-austenite interface at a cell boundary triple point. This corresponds to the eutectic ferrite structures shown in Fig. 2 and the primary austenite solidified regions of welds in alloy 19-11 as shown in Fig. 3A.

Figure 6B shows sulfide particles along both the skeletal ferrite-austenite interface and within the solidification cell boundary. This ferrite structure corresponds to some of the ferrite of alloy 19-11, and to most of the ferrite of alloy 22-13 shown in Fig. 3B and the skeletal ferrite shown schematically in Fig. 2. Figure 6C shows sulfides at ferrite lath tips. This structure was characteristic of alloy 23-12 and corresponds to the tips of laths near the cell boundaries shown schematically in Fig. 2, and in the micrograph of Figure 3C.

The EDS (energy dispersive spectroscopy) spectrum taken in the STEM analysis of the sulfide particles is shown in Fig. 6D. This spectrum is from the CrS particle shown in Figure 6A but is characteristic of all the particles shown in Fig. 6. S could not be detected in solid solution in either ferrite or austenite with STEM analysis due to detection limitations.

Chromium phosphide particles were also observed along the eutectic ferrite-austenite interphase boundaries and ferrite-free cell boundaries of P-doped alloys. Some phosphides (0.1μm in size) were also observed along skeletal ferrite-austenite interfaces, but only at high levels of P (P > 0.2%). The observed phosphide particles appeared from TEM elec-

**Table 2—Comparison of Calculated Impurity Additions vs. Chemical Analysis of Test Welds**

| Weld | Impurity | Analysis, wt-% | Calculated addition, wt-% |
|---|---|---|---|
| 23-12 | S | 0.054 | 0.067 |
| 21-14 | S | 0.069 | 0.085 |
| 10-30 | S | 0.058 | 0.065 |
| 21-14 | S | 0.027 | 0.020 |
| 19-11 | S | 0.027 | 0.042 |
| 10-30 | P | 0.052 | 0.028 |
| 19-11 | P | 0.183 | 0.17 |
| 23-12 | P | 0.128 | 0.010 |

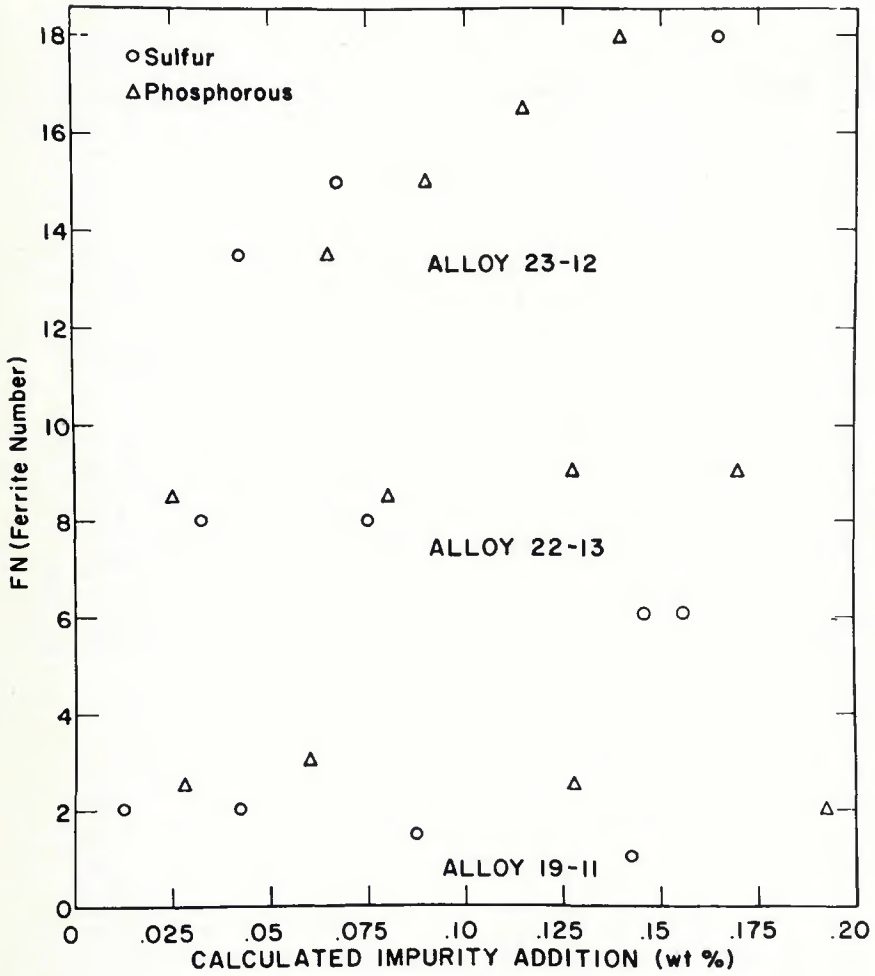


*Fig. 5—Measured ferrite contents of spot Varestraint test welds doped with P and S*

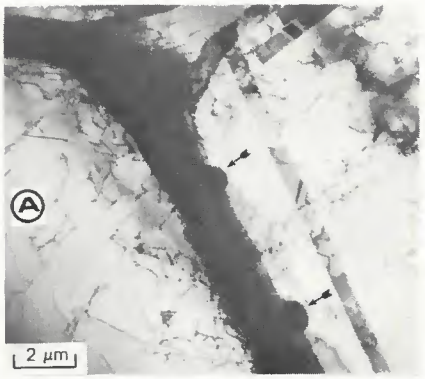


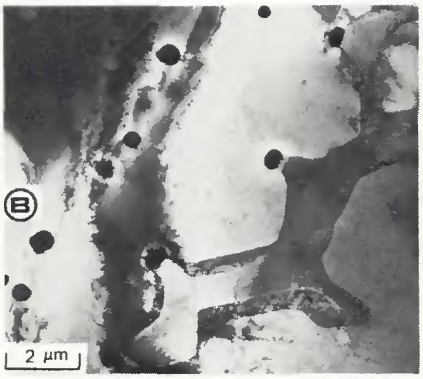


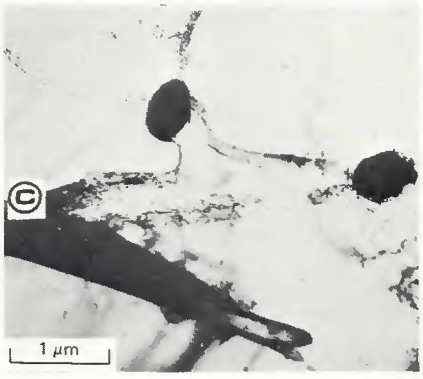


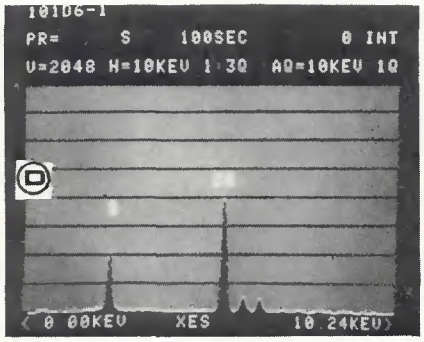


*Fig. 6—TEM micrographs: A—sulfides at eutectic ferrite-austenitic boundary; B—sulfides along skeletal ferrite-austenitic boundary and within cell boundary; C—sulfides at ferrite lath tips; D—STEM EDS spectrum of CrS particles*

tron diffraction studies and STEM analysis to be CrP. Unlike sulfides in S doped samples, phosphide particles were not observed in TEM along lath boundaries in samples containing lathy ferrite.

Also unlike S, P could be detected in solid solution in all ferrite morphologies. The measured P levels were always higher in ferrite than austenite and were, in general, maximum in the ferrite adjacent to the $\delta$-$\gamma$ boundaries.

The higher solubilities of P compared to S in both ferrite and austenite, and the formation of CrP vs. CrS would be consistent with the smaller volume fraction of phosphide than sulfide particles observed at equivalent levels of doping.

## Rationale for Changes in Ferrite Content

It seems likely that alloying additions act as Cr or Ni equivalents by serving as either ferrite or austenite formers, in which case they influence the relative amounts of primary and secondary solidification of ferrite and austenite. In addition, elemental partitioning during the solid state transformation of $\delta \rightarrow \gamma$ in primary ferrite solidified welds will preferentially stabilize one of the phases. However, in this study it was observed that S and P had varying, and sometimes opposite, effects on welds of the three alloys studied.

The formation of CrS can be expected to reduce the ferrite content by removing Cr from solid solution. If all the S is present as CrS, one may predict from atomic weights of $Cr_{eq} \sim -1.6$ for S. Using this assumption, at FN $\sim 2$ on the DeLong diagram (Fig. 1), a reduction of ferrite resulting from a 0.2% S addition is predicted to be $\sim 1$ FN. This is in relatively good agreement with the data of alloy 19-11 shown in Fig. 5.

P had little effect on the measured ferrite content of welds in alloy 19-11. However, since the phosphides are apparently $CrP_3$, and the atomic weights of P and S are similar, one would predict, other things being equal, that P would only be $\sim \frac{1}{3}$ as effective as S in reducing the Cr, and thus ferrite content. Moreover, the solubility of P is greater than that of S in both ferrite and austenite (Ref. 26), further decreasing the relative potency of P in withdrawing Cr from solution

by forming $CrP_3$. Therefore, even though the P can reduce the ferrite content by combining with Cr, the amount of reduction at only ~0.2% P (~0.3 FN) would not be evident within the experimental scatter. The above factors can explain the small but measurable amount of ferrite reduction with S additions and the almost undetectable effect of P in alloy 19-11.

In alloy 23-12, both P and S significantly increased the measured levels of ferrite. Thus, even though the formation of CrS and $CrP_3$ should reduce the ferrite content, this effect must be overridden by another factor. Since P and S were not observed to act as Cr equivalents in alloys 19-11 and 22-13, the significant increase in FN in alloy 23-12 shown in Fig. 5 would seem difficult to explain. The $Cr_{eq}$ factor of both S and P calculated in the same manner as above, except now for alloy 23-12 at 14-18 FN, is $Cr_{eq}$ ~7 at the impurity levels studied.

It is well known that in welds containing the lathy ferrite morphology, a large fraction of the structure solidifies as primary ferrite. Upon cooling, most of the ferrite transforms to austenite by a diffusion-controlled transformation (Ref. 10,21,22). Some indication of the mechanism by which S increased the ferrite content by retarding the transformation is shown in the TEM micrographs in Fig. 6B and 6C; evidence of sulfides pinning the interphase boundary of the skeletal ferrite is shown in Fig. 6B. However, a high density of sulfide particles is also evident along the ferrite-free cell boundary. Pinning of the lathy ferrite structure by CrS is shown in Fig. 6C. In both these structures, the pinning of the boundaries means that the growing austenite during cooling cannot consume as much ferrite as when boundaries are unpinned, thereby producing a net increase in ferrite content. Since S could not be detected in solid solution in either the ferrite or austenite phases, S is probably not thermodynamically stabilizing the ferrite phase.

P was detected in solid solution in both ferrite and austenite, but partitions preferentially to the ferrite (Ref. 10,26). It was determined by STEM analysis that P content was maximum in the ferrite adjacent to the $\delta$-$\gamma$ interphase boundary, resulting from the rejection of P from the austenite during the $\delta \rightarrow \gamma$ transformation (Ref. 10). As mentioned above, phosphides were not observed in TEM along the lath boundaries of small castings doped with 0.2% P. However, some small phosphide particles were observed along the $\delta$-$\gamma$ interphase boundaries of skeletal ferrite in small castings of alloy 22-13 doped with 0.2% P. Since P stabilizes the ferrite (Ref. 26), P possibly reduces the transformation of $\delta \rightarrow \gamma$ by thermodynamically stabilizing the ferrite adjacent to the interphase boundary where the concentration of rejected P is maximum. This would further act to reduce the mobility of the boundary, in addition to the pinning action of any small phosphide particles which may occur at high P levels along the phase boundary.

In alloy 22-13, P slightly increased the measured ferrite level. However, at high S levels (~0.15%) the measured ferrite content significantly decreased. Although this alloy solidified as primary ferrite, the same as alloy 23-12, the ferrite exhibits primarily the skeletal morphology rather than the lathy ferrite of alloy 23-12. The difference in behavior of alloys 23-12 and 22-13 may be partially related to the degree of primary ferrite solidification and the temperature range of the solid state transformation. A larger fraction of solidification as ferrite would occur in alloy 23-12 than in alloy 22-13 because the latter is situated closer to the eutectic trough of the Fe-Ni-Cr ternary diagram. This is also shown schematically in Fig. 2.

The amount of primary ferrite solidification could have an effect on the degree of interphase boundary pinning; most of the CrS particles were observed in the cell boundaries. The highest concentration of P and S in solid solution would also be expected in the cell boundary regions due to partitioning during solidification. Thus in the lathy ferrite-containing welds of alloy 23-12, both sulfide particles and impurities in solid solution would be expected to interact with the $\delta$-$\gamma$ boundary, because solidification occurred almost 100% as ferrite. In welds of alloy 22-13, more secondary austenitic solidification occurred, leaving many of the particles and high P and S impurity concentrations in austenitic cell boundaries outside of the ferrite-austenite interface. In this case, the phase boundaries would be more free to migrate during the solid state transformation. This rationale is also consistent with the structures shown in Fig. 6B and 6C.

The transformation resulting in the skeletal morphology also occurs, in general, at compositions which have lower $Cr_{eq}/Ni_{eq}$ ratios (Ref. 19) and which thus lie closer to the ternary eutectic trough than do the chemistries of lathy ferrite-containing welds. These compositions will enter the ($\delta$+$\gamma$) two phase fields at higher transformation temperatures where both the atomic mobilities are greater and longer times are available for the transformation to occur. These factors may also account for the less apparent pinning of the skeletal ferrite than that of the lathy ferrite structure.

From the data in Fig. 5, it appears that P may reduce the boundary mobility resulting in slightly increased skeletal ferrite contents of the welds of alloy 22-13, while the reduction of Cr by the formation of CrS overrides the effect of reduced boundary mobility that results from segregation of S or pinning by CrS.

In welds of alloy 19-11 which solidify in a mixed mode, evidently little pinning results during the transformation of the primary ferrite solidified regions. This conclusion is based on the fact that the change in ferrite with increasing sulfur is close to that predicted by the reduction of Cr in solution by the formation of CrS. STEM analysis of primary austenitic solidified welds indicated that little, if any, of the eutectic ferrite transformed to austenite upon cooling (Ref. 10,21,23); therefore, pinning of this structure would be minimal. However, some transformation of ferrite to austenite may be expected with slower cooling rates.

## Conclusion

Alloying elements may act as $Cr_{eq}$ or $Ni_{eq}$ by affecting the structure or degree of primary solidification, or by preferentially stabilizing the ferrite or austenite by partitioning during the solid state transformation. Also, alloying elements or impurities may act in a synergistic fashion. For example, strong $Ni_{eq}$ elements such as C and N may be removed from solution by compound formation (Ref. 27).

In alloys studied in this investigation, P and S were found to have varying effects, depending upon weld structure. In primary austenite solidified welds, P and S were found to reduce the ferrite content by reducing the Cr content through the formation of CrS and $CrP_3$. These phases form primarily during the solidification process. However, in primary ferrite solidified welds, this effect may be overridden by the action of $CrP_3$ and CrS in restricting mobility of the $\delta \rightarrow \gamma$ interphase boundaries by acting as pinning sites. Also, P and S in solid solution segregate to the ferrite phase during the solid state transformation. These higher impurity concentrations, especially in the near-boundary region, may further stabilize the ferrite phase, or may retard the transformation kinetics, resulting in a net increase in ferrite content.

It should also be pointed out that in Mn-containing alloys, such as in commercial stainless steels, the formation of MnS in preference to CrS would tend to increase the ferrite content by conserving Cr in solid solution, rather than reducing it as may happen when CrS forms. However, when interphase boundary pinning is the process affecting ferrite content, the effect for both sulfides may be expected to be similar. It must be recognized that the P and S contents used in this study are much higher than those typical of the AISI 300 series alloys. Also, the varying effect of these elements on ferrite content would further preclude their incorporation in diagrams used for predicting ferrite.

*Acknowledgments*

The experimental assistance of R. Bell of Sandia National Laboratories with Varestraint specimen preparation and testing is greatly appreciated. This work

was sponsored jointly by the Center of Joining of Materials at Carnegie-Mellon University and by the Department of Energy under Contract No. DE-AC04-76DP00798.

*References*

1. Scherer, R., Riedrich, G., and Hougardy, H. 1941 (May 6). *Welding rod.* U. S. Patent 2,240,672.

2. Hull, F. C. 1967. Effect of delta ferrite on the hot cracking of stainless steel. *Welding Journal* 46(9):399-s to 409-s.

3. Schaeffler, A. L. 1949. *Metals Progress* 56:680.

4. DeLong, W. T., Ostrom, G. A., and Szumachowski, R. R. 1956. Measurement and calculation of ferrite in stainless-steel weld metal. *Welding Journal* 35(11):521-s to 528-s.

5. Hull, F. C. 1973. Delta ferrite and martensite formation on stainless steels. *Welding Journal* 52(5):193-s to 203-s.

6. Borland, J. C., and Younger, R. N. 1960. Some aspects of cracking in welded Cr-Ni austenitic steels—a survey of the literature. *British Welding Journal* 7(1):22-59.

7. Brooks, J. A., Thompson, A. W., and Williams, J. C. 1980. *Physical metallurgy of metal joining,* eds. R. Kossowsky and M. Glicksman, pp. 117-136. TMS, AIME.

8. Masumoto, I., Tamaki, K., and Kutsuna, M. 1972. *Trans. JWS* 41(11):1306-1314.

9. Thier, H. 1976. *DVS-Ber.* 41:100-104.

10. Brooks, J. A. 1981 (April). *Composition effects on the microstructure and cracking of austenitic stainless steel welds.* PhD thesis, Carnegie-Mellon University.

11. Turner, P. W., and Lundin, C. D. 1970. Effect of hot cracking of uranium weld metal—part I. *Welding Journal* 49(12):579-s to 587-s.

12. Kujanpää, V., Suutala, N., Takalo, T., and Moisio, T. 1979. *Welding Research Inter.* 9(2):55-76.

13. Lyman, C. E., Manning, P. E., Duquette, D. J., and Hull, E. 1978. *Scanning electron microscopy,* vol. 1, pp. 213-220.

14. Lippold, J. C., and Savage, W. F. 1979. Solidification of austenitic stainless steel weldments: part I—a proposed mechanism. *Welding Journal* 58(12):362-s to 374-s.

15. Lippold, J. C., and Savage, W. F. 1981 (August). Modeling solute distribution during solidification of austenitic stainless steel weldments. *TMS-AIME proceedings—casting and welding process modeling,* Rindge, New Hampshire.

16. Savage, W. F. 1980. 1980 Houdremont lecture: Soldification, segregation and weld imperfections. *Welding in the World* 18(5/6):89-113.

17. Fredriksson, H. 1972. Met. Trans. 3(11):2989-97.

18. David, S. A., Goodwin, G. M., and Braski, D. N. 1979. Solidification behavior of austenitic stainless steel filler metals. *Welding Journal* 58(11):330-s to 336-s.

19. Suutala, N., Takalo, T., and Moisio, T. 1979. *Met. Trans. A* 10(8):1183-1190.

20. David, S. A. 1981. Ferrite morphology and variations in ferrite content in austenitic stainless steel welds. *Welding Journal* 60(4):63-s to 71-s.

21. Brooks, J. A., Williams, J. C., and Thompson, A. W. 1981. Solidification and solid state transformations of austenitic stainless steel. *Trends in welding research in the United States,* pp. 331-355. Metals Park, Ohio: American Society for Metals.

22. Brooks, J. A., Williams, J. C., and Thompson, A. W. 1983 (July). Microstructural origin of the skeletal ferrite morphology of austenitic stainless steel welds. *Met. Trans. A.*

23. Brooks, J. A., Williams, J. C., and Thompson, A. W. 1983. STEM analysis of primary austenite solidified stainless steel welds. *Met. Trans. A* 14(1):23-31.

24. Thompson, R. D. Jr. 1978 (Dec. 10-15). In ASME winter conf. proc., *Critical materials and fabrication issues for pressure vessels, piping, pumps and valves,* sponsored by ASME and HBS, San Francisco, California.

25. Goodwin, G. M., Cole, N. C., and Slaughter, G. M. 1972. A study of ferrite morphology in autenitic stainless steel weldments. *Welding Journal* 51(9):425-s to 429-s.

26. Hansen, M. 1958. *Constitution of binary alloys.* New York: McGraw Hill Company.

27. Allen, R. M. Unpublished research. Livermore, California: Sandia National Laboratories.

## *A REMINDER TO AUTHORS—*

*If you plan to present a paper at the AWS 65th Annual Meeting April 9–13, 1984, be sure to get your abstract with the Author Application Form (opposite page 146-s May issue) into the mail no later than August 15, 1983.*

*For papers to be presented at the 15th International AWS-WRC Brazing and Soldering Conference, April 10–12, 1984, the Author Application Form (opposite page 58-s, February) and abstract must also be mailed no later than August 15, 1983.*

# WRC Bulletin 279
# July, 1982

### Weldability and Fracture Toughness of Quenched and Tempered 9% Nickel Steel: Part I—Weld Simulation Testing
**by A. Dhooge, W. Provost and A. Vinckier**

An investigation on the weldability of a quenched and tempered 9% Ni steel using weld simulation and artificial aging to estimate the heat-affected zone ductility at cryogenic temperatures is reported in Part I. Charpy-V bars were subjected to various weld simulation cycles and subsequent heat treatments and, after notching, broken at a range of cryogenic temperatures.

### Weldability and Fracture Toughness of Quenched and Tempered 9% Nickel Steel: Part II—Wide Plate Testing
**by A. Dhooge, W. Provost and A. Vinckier**

In addition to standard impact and tensile tests, a large number of wide plate specimens welded with various consumables and welding processes were tested to evaluate the toughness and defect acceptability of 9% Ni steel in plate thicknesses greater than 25 mm.

Publication of these reports was sponsored by the Weldability Committee of the Welding Research Council.

The price of WRC Bulletin 279 is $10.00 per copy, plus $3.00 for postage and handling. Orders should be sent with payment to the Welding Research Council, 345 East 47th St., New York, NY 10017.

# WRC Bulletin 281
# October, 1982

### Hydrodynamic Response of Fluid Coupled Cylinders, Simplified Damping and Inertia Coefficients
**by S. J. Brown**

This study presents the development of the concept of inertia and damping coefficients in an historical context with experimental, classical and numerical investigations into the dynamics of fluid coupled cylinders. It is shown that coefficients may be used to account for coaxial cylinder end conditions, eccentricity, skewness, clusters, shell modes and axial modes.

Publication of this report was sponsored by the Subcommittee on Dynamic Analysis of Pressure Components of the Pressure Vessel Research Committee of the Welding Research Council.

The price of WRC Bulletin 281 is $11.50 per copy, plus $3.00 for postage and handling (foreign + $5.00). Orders should be sent with payment to the Welding Research Council, 345 E. 47th St., Room 1301, New York, NY 10017.

# WRC Bulletin 282
# November, 1982

### Elastic-Plastic Buckling of Axially Compressed Ring Stiffened Cylinders—Test vs. Theory
**by D. Bushnell**

Concern for the safety of nuclear plants and offshore structures has stimulated efforts to determine buckling characteristics of stiffened cylindrical steel shells.

In this paper, BOSOR 5 computer programs were used to predict buckling loads of forty axially compressed mild steel cylindrical shells previously tested at Chicago Bridge & Iron Co.

Publication of this report was sponsored by the Subcommittee on Shells of the Pressure Vessel Research Committee of the Welding Research Council.

The price of WRC Bulletin 282 is $10.75 per copy plus $3.00 for postage and handling (foreign + $5.00). Orders should be sent with payment to the Welding Research Council, 345 E. 47th St., Room 1301, New York, NY 10017.